Optimal Operation of an Industrial-Scale Parex Process for the Recovery of p-Xylene From a Mixture of C8 Aromatics

ARTICLE *in* INDUSTRIAL & ENGINEERING CHEMISTRY RESEARCH · JULY 2005

Impact Factor: 2.59 · DOI: 10.1021/ie0488694

3 AUTHORS, INCLUDING:

Ajay Ray
The University of Western Ontario

175 PUBLICATIONS **4,983** CITATIONS

SEE PROFILE

Optimal Operation of an Industrial-Scale Parex Process for the Recovery of *p*-Xylene from a Mixture of C_8 Aromatics

Anjushri S. Kurup, K. Hidajat, and Ajay K. Ray*

Department of Chemical and Biomolecular Engineering, National University of Singapore, 4 Engineering Drive 4, Singapore 117576

Multi-objective optimization for the operation and design of an industrial-scale Parex process for the recovery of *p*-xylene from a mixture of C_8 aromatics has been studied using a state-of-the-art optimization technique: the Elitist Nondominated Sorting Genetic Algorithm with Jumping Genes (NSGA-II-JG, binary coded). An industrial-scale Parex process, which is based on simulated moving bed (SMB) technology, was simulated using an available mathematical model. The simulation results were verified with the reported industrial data. Subsequently, few two-objective optimization problems were solved to determine the optimum number of columns, the length of each column, and the column distribution in different zones. Significant improvement in the recovery of *p*-xylene using less solvent was obtained when a suitable column length and appropriate distribution of columns in various zones was chosen. Optimization study was also extended for the Varicol operation mode, which is based on a nonsynchronous switching, contrary to the synchronous switching used in traditional SMB systems. It was observed that the performance of the Varicol process is much superior to that of a SMB process, in terms of recovering more *p*-xylene while consuming less eluent. Results are presented and discussed in detail. The optimum results are also explained using equilibrium theory by locating them in the pure separation region.

Introduction

The Parex process is an innovative adsorptive separation method for the recovery of *p*-xylene (1,4-dimethyl benzene) from a mixture of C_8 aromatic isomers (consisting of ethyl benzene, as well as *o*-xylene, *m*-xylene, and *p*-xylene). The boiling points for these isomers are so similar that separating them via conventional distillation is not practical. The primary end use of *p*-xylene is for the production of fibers, films, or resins, including polyester fibers that are used for household fabrics, carpets, and clothing. This is accomplished through the oxidation of the *p*-xylene to terephthalic acid (TPA) or dimethyl terephthalate (DMT), which are then reacted with ethylene glycol to produce poly(ethylene terephthalate) (PET). PET is a raw material for most polyesters. The use of polyester films and fibers is increasing rapidly, mainly in the Pacific Rim countries.

The Parex process is a continuous process based on simulated moving bed (SMB) technology.[1] SMB helps to achieve the separation performance of a true moving bed while avoiding the difficulties in the movement of a solid phase. Separation is achieved by exploiting the differences in affinity of the adsorbent (e.g., solid zeolitic adsorbent) that is selective for *p*-xylene and is designed to recover >97 wt % of the *p*-xylene from the feed in a single pass while delivering a product purity of ≥99.9 wt %. The SMB technique implies a simulated countercurrent contact between the mobile fluid phase and the stationary adsorbent phase. There are many advantages of the SMB technology,[2] compared to the classical preparative chromatography, namely, overcoming problems associated with solid handling, efficient utilization of adsorbent/catalyst, continuous mode of operation, a reduction in solvent consumption (with up to 90% savings, compared to classical preparative chromatography), a reduction in downtime (because separation and regeneration occur concurrently), the possibility of scaling up to a large-scale production unit (because of the simplicity in the mechanical design), etc. A schematic representation of a SMB system is illustrated in Figure 1, which consists of a number of packed (with adsorbent) columns of uniform cross-section connected in a circular array, each of length L_{col}. The two incoming streams (the feed F, and the desorbent D) and the two outgoing streams (the raffinate Ra, and the extract Ex) divide the system into four sections (zones), namely P, Q, R, and S, each of which is comprised of p, q, r, and s columns, respectively. The flow rates in sections P, Q, R, and S are designated as Q_P, Q_Q, Q_R, and Q_S, respectively, whereas those of the feed, raffinate, desorbent, and extract are designated as Q_F, Q_{Ra}, Q_D, and Q_{Ex}, respectively. However, only four of the aforementioned eight flow rates are independent; the remaining four are determined from the mass balance at points (nodes) A, B, C, and D (see Figure 1). Even though the Parex process works on the same principle as that shown in Figure 1, the actual configuration is somewhat different (see Figure 2). In this case, the adsorbent is not contained in discrete columns (beds) separated by switch valves; instead, they are contained in a single bed that is divided into a number of segments. The introduction and withdrawal of fluid from each segment

* Corresponding author. Contact details (starting July 1, 2005): Department of Chemical and Biochemical Engineering, University of Western Ontario, London, Ontario N6A 5B9, Canada. Tel: +1 519 661 2111. Fax: +1 519 661 3498. E-mail: aray@eng.uwo.ca.

10.1021/ie0488694 CCC: $30.25
Published on Web 06/23/2005

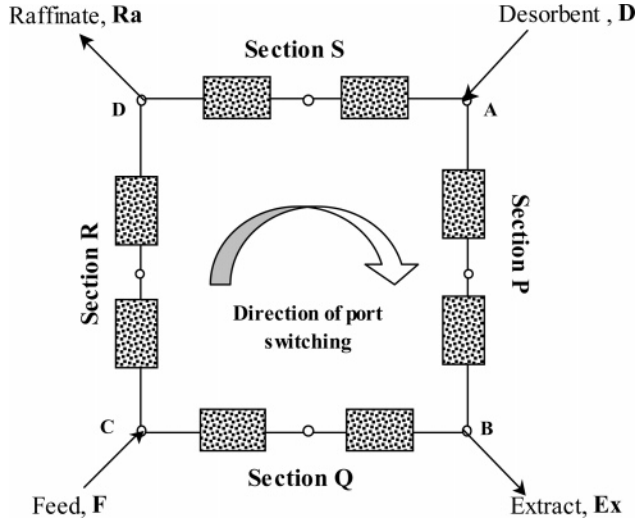

Figure 1. Schematic diagram of an eight-column simulated moving bed (SMB) system.

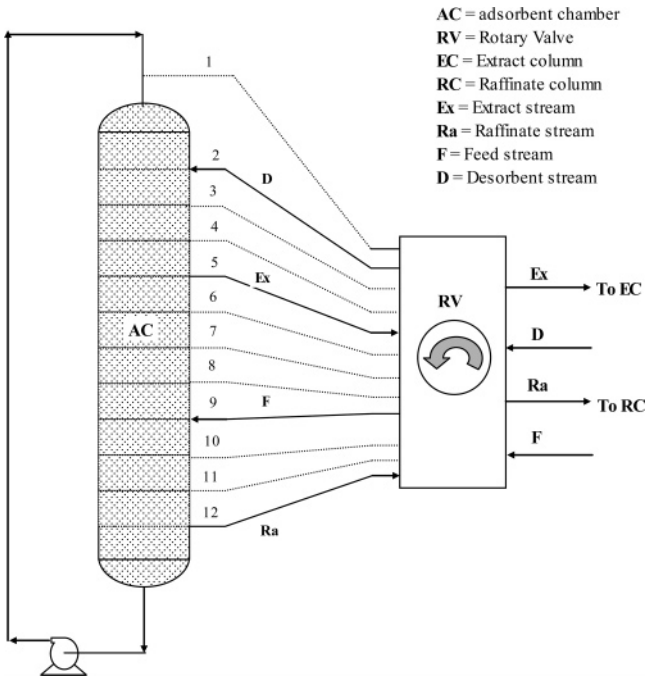

Figure 2. Schematic flow diagram showing the operation of the Parex process.

is performed by specially designed flow distributors. A pump recirculates fluid from the bottom to the top of the column. At any time, only four of the connections to the packed bed are utilized. A rotary valve connected to each stream advances the two inlet and the two outlet points (feed, desorbent, extract, and raffinate) by one segment in the direction of fluid flow and thus simulates the solid motion in the opposite direction. The valve also passes the extract and the raffinate streams to the respective ancillary distillation columns to remove the desorbent, which is recycled back to the process.[2]

Recently, the Varicol process,[3] which is a modification of SMB technology, is also being widely addressed, because of its enhanced performance, compared to SMB. In the Varicol operation,[3] a nonsynchronous shift of the inlet and outlet ports is used within a switching period contrary to the synchronous switching scheme used in the SMB system. The switching period and sequence is decided a priori and maintained constant. During one global switching period, there are different column configurations for sub-time intervals, because of the local switching. Given the total number of columns used in a Varicol process, the number of columns in each zone varies with time within a global switching period. However, the number of columns in each zone recovers to the starting value at the end of the global switching period and the aforementioned switching process is repeated. Therefore, the locations of input/output ports (note that a port is implied at the beginning/end of each column in each section) in the Varicol process are quite different from those of the SMB process, because the ports are not shifted concurrently. Moreover, a port may shift more than once during one global switching period, either in the forward direction or even in the backward direction. As a result, the Varicol process can have several column configurations, which gives it more flexibility, compared to the more-rigid traditional SMB process. Note that the Varicol process does not add any additional fixed cost. Application as well as rigorous optimization of this particular mode of operation has been extensively studied for various separation processes,[4,5] including reactive separation processes.[6,7] The details of the Varicol operation can be obtained elsewhere.[3−7]

Several other industrial processes for the separation of the C_8 aromatic isomers have been developed in the past. These are usually coupled with an isomerization process that is intended to transform some or all of the other isomers into *p*-xylene. The earliest processes for the separation of these C_8 aromatic isomers were based on crystallization.[8] The adsorption of xylenes on ion-exchanged faujasite-type zeolites have been studied extensively in the liquid,[9−13] as well as in the vapor phase.[14−20] A detailed analysis of the design and optimization of a four-section SMB unit for separation of this C_8 aromatic mixture operating on liquid and vapor phases has been presented by Storti et al.,[21] in which appropriate flow-rate ratios for each section were established from equilibrium theory. An industrial-scale SMB unit for the separation of the same was studied by Minceva and Rodrigues[22] through simulation studies.

Despite being such an old and established industrial process, there is no work reported in the open literature that involves the rigorous optimization of the Parex process. The performance of the SMB (as well as the Varicol) process is strongly dependent on the complex interplay of different operating, as well as design, parameters. The optimization problem is complicated by the relatively large number of decision variables, including continuous variables, such as flow rates and lengths, as well as discontinuous variables, such as column number and configuration. Moreover, it is important to reformulate the optimization problem as multiobjective,[23] because, usually, the factors that affect the economy of a given separation process are multiple and are often in conflict with each other. A typical example is the maximum recovery of *p*-xylene using minimum solvent. The principle of multicriterion optimization with conflicting objectives is different from that of single objective optimization. Instead of trying to find the unique and best (global) optimum design solution, the goal of multiobjective optimization is to find a set of equally good solutions, which are known as Pareto optimal solutions.[23,24] A Pareto set is such that, when one moves from any one point to another within the set, at least one objective function improves while at least one other deteriorates. The importance of multiobjective

Table 1. Details of the Industrial Parex Unit, along with Model Parameters and Operating Conditions[a]

parameter	value
SMB Unit Geometry	
N_{col}	24
L_{col}	1.135 m
d_{col}	4.117 m
Ω	6/9/6/3
V_c	15.1 m^3
Operating Conditions	
T	453 K (liquid phase)
t_s	1.16 min
Q_F	1.45 m^3/min
Q_{Ex}	1.65 m^3/min
Q_{Ra}	2.69 m^3/min
Q_D	2.89 m^3/min
Q_S	5.39 m^3/min
Model Parameters	
Pe	2000
k_h	2 min^{-1}
d_p	9.2×10^{-4} m
ϵ	0.39
ρ	1.39×10^3 kg/m^3
$q_{m_{PX(m-X;o-X;EB)}}$	0.1303 kg/kg
K_{pX}	1.0658 m^3/kg
K_{m-X}	0.2299 m^3/kg
K_{o-X}	0.1884 m^3/kg
K_{EB}	0.3037 m^3/kg
$q_{m_{pDEB}}$	107.7 kg/kg
K_{pDEB}	1.2935 m^3/kg

[a] Data taken from ref 22.

optimization and the improvement in performance achieved in the SMB and Varicol processes for various applications have been studied systematically in the literature[25−27] and are not reported here, for the sake of brevity.

In this paper, multiobjective optimization study is performed for the Parex process. The industrial data provided by Minceva and Rodrigues[22] were used for verification of the mathematical model. The feed is considered to be a typical C_8 aromatics mixture containing 23.6% *p*-xylene, 49.7% *m*-xylene, 12.7% *o*-xylene, and 14% ethylbenzene. Completely potassium-exchanged Y-zeolite is used as the adsorbent, whereas the desorbent used is solvent *p*-diethyl benzene (*p*DEB). Toluene can also be used as a desorbent for this separation process. However, *p*DEB is less volatile than the xylene isomers.[2] This is very advantageous because, in the ancillary product separation, the desorbent is recovered as the bottom product, and, because the desorbent is generally in excess, this reduces the heat load on the distillation column. This leads to a more economical process operation. Details of the other operating conditions and design parameters are listed in Table 1. The optimization study is directed toward improving the recovery of *p*-xylene, using minimum solvent consumption. Furthermore, by comparing the performance of the Varicol process with an equivalent SMB process, this work tries to determine to what extent operation of a SMB system can be improved by applying nonsynchronous switching with varying zone lengths.

Mathematical Model

As discussed previously, in SMB, the counter-current motion of fluid and solid is mimicked by a discrete shifting of injection and collection points in the direction of the fluid phase. The SMB system then consists of a set of identical fixed-bed columns, which are connected in series. Model equations for the SMB result from the mass balance over a volume element of the bed and inside the particle. Axial dispersion for the bulk fluid phase is included and the linear driving force approximation is used to describe the intraparticle mass-transfer rate. The mathematical model used here is similar to that described by Pais et al.[28] The differential transient mass balance equations, along with the boundary conditions, are as follows:

$$\frac{\partial C_{i,k}}{\partial \theta} + \upsilon \frac{\partial \bar{q}_{i,k}}{\partial \theta} = \frac{\psi_k}{Pe_k} \frac{\partial^2 C_{i,k}}{\partial \chi^2} - \psi_k \frac{\partial C_{i,k}}{\partial \chi} \tag{1}$$

$$\frac{\partial \bar{q}_{i,k}}{\partial \theta} = \alpha(\bar{q}^*_{i,k} - \bar{q}_{i,k}) \tag{2}$$

The nonstoichiometric Langmuir isotherm was used to describe the multicomponent adsorption equilibria:

$$\bar{q}^*_{i,k} = \frac{q_{mi} K_i C_{ik}}{1 + \sum_{l=1}^{NC} K_i C_{lk}} \tag{3}$$

where $\chi = z/L_{col}$ and $\theta = t/t_s$. The boundary conditions are

$$C^{in}_{i,\chi} = C_{i,k}(0,\theta) - \frac{1}{Pe_k} \frac{\partial C_{i,k}}{\partial \chi} \tag{4}$$

$$\frac{\partial C_{i,k}}{\partial \chi}(1,\theta) = 0 \tag{5}$$

The initial conditions are given as

$$C_{i,k}(\chi,0) = C^0_{i,k}(\chi) \tag{6a}$$

and

$$\bar{q}_{i,k}(\chi,0) = \bar{q}^0_{i,k}(\chi) \tag{6b}$$

The dimensionless parameters used in the aforementioned equations are given as

$$\psi_k = \frac{U_{F_z} t_s}{L_{col}} \tag{7a}$$

$$\alpha = k_h t_s \tag{7b}$$

and

$$Pe_k = \frac{U_{F_k} L_{col}}{D_{axk}} \tag{7c}$$

The mass balance at the node is then

$$C^{in}_{i,k} = C_{i,k-1}(1,\theta) \tag{8}$$

except if the column follows feed or desorbent port. In that case,

$$C^{in}_{i,k} = \frac{Q_F C_{i,F} + Q_S C_{i,k-1}(1,\theta)}{Q_P} \tag{9a}$$

Table 2. Comparison of Simulation Results Obtained to Reported Literature

method	Rec_pX (%)	Pur_pX (%)	CPU time (min)	platform
Method of Lines, MOL[a]	98.16	98.96	18.5	Cray J916
Orthogonal Collocation on Finite Elements, OCFE[a]	98.29	99.51	1.2	Cray J916
general process modelling system, gPROMS[b]	98.2	99.78	510	Pentium III

[a] From this work. [b] Results reported by Minceva and Rodrigues[22] using gPROMS, which is a general purpose process modeling, simulation, and optimization software program.

and

$$C_{i,k}^{\text{in}} = \frac{Q_Q C_{i,k-1}(1,\theta)}{Q_R} \tag{9b}$$

respectively. These equations are then slightly modified to account for the changes involved in the Varicol operation. The details pertaining to the adsorption isotherms and the experimental setup are summarized in Table 1. The equilibrium data for *o*-xylene, *m*-xylene, *p*-xylene, ethyl benzene, and *p*-dimethylbenzene at 453 K were taken from the work of Azevedo et al.[12]

Two different numerical solution approaches were used to solve these set of partial differential equations (PDEs), along with their boundary conditions. In the first method, the PDEs were discretized in space using the Finite Difference Method (FDM) to convert them into a system of coupled ODE−IVPs (Method of Lines, MOL).[29] The number of theoretical plates used was 50. These stiff initial value ODEs were solved using the subroutine, DIVPAG (based on Gear's method), in the IMSL library. In the second approach, an Orthogonal Collocation on Finite Elements (OCFE) method was used to discretize the axial domain. In this case, each column was divided into six equal finite elements and each element was discretized with two internal collocation points to convert them again to a system of coupled ODE−IVPs, as done previously. These were again solved using the subroutine DIVPAG subroutine of the IMSL library. Because periodic switching is imposed on the system, the separators always work under transient conditions. However, a cyclic (periodic) steady state with a period equal to the global switching time is eventually reached after several switching. For both the SMB and Varicol processes, the periodic steady state was attained after about 40 switching cycles around the unit. Table 2 compares the simulation results obtained using the two numerical approaches used in this study with simulation results reported by Minceva and Rodrigues.[22] The operating conditions used for all these simulation runs are the same as that reported in Table 1. Table 2 also shows the computational time taken for one simulation run by each method. The simulations in our study were performed on a Cray J916 supercomputer. The table clearly shows that the OCFE method works much faster than that of the MOL method, which is understandable, because of the drastic reduction in the total number of equations in the former case. Figure 3 compares the steady-state internal concentration profiles obtained using the two numerical methods for the parameter values listed in Table 1. The separation performance was evaluated by calculating the recovery (Rec) and purity (Pur) achieved at the extract port,

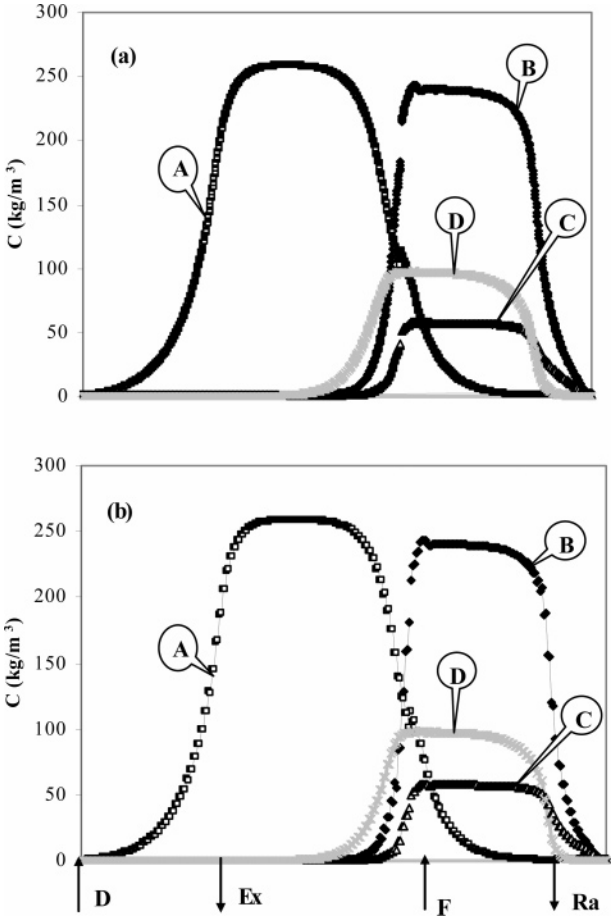

Figure 3. Comparison of steady-state concentration profiles for different components for simulation of industrial point (see Table 1 for data) obtained from two different numerical solution techniques (namely, Method of Lines (MOL) and Orthogonal Collocation on Finite Elements (OCFE). Legend is as follows: A, *p*-xylene; B, *m*-xylene; C, *o*-xylene; and D, ethyl benzene.

because the objective in the Parex process is to obtain pure *p*-xylene. These quantities were defined as follows:

Purity of *p*-xylene in the extract (%):

$$\text{Pur\_pX} = \frac{C_{\text{Ex}}^{\text{pX}}}{C_{\text{Ex}}^{\text{pX}} + C_{\text{Ex}}^{\text{mX}} + C_{\text{Ex}}^{\text{oX}} + C_{\text{Ex}}^{\text{EB}}} \times 100 \tag{10}$$

and

Recovery of *p*-xylene (%):

$$\text{Rec\_pX} = \frac{C_{\text{Ex}}^{\text{pX}} Q_{\text{Ex}}}{C_{\text{F}}^{\text{pX}} Q_{\text{F}}} \times 100 \tag{11}$$

The emphasis of this study is on performing a rigorous multiobjective optimization of the Parex process in recovering high-purity *p*-xylene from the C_8 aromatic mixture, using an adaptation of Genetic Algorithm. To obtain global Pareto optimal solution, one must perform

Table 3. Description of the Multiobjective Optimization Problems Solved in This Study

problem	objective function	decision variables	constraints	fixed parameters
1a (SMB)	Max Rec_pX, Min Q_D	1 min $\le t_s \le$ 2 min; 2 m^3/min $\le Q_{Ra} \le$ 3 m^3/min; 2 m^3/min $\le Q_D \le$ 3.5 m^3/min; 1 m $\le L_{col} \le$ 1.15 m	Rec_pX $\ge$ 92%, Pur_pX $\ge$ 98%	d_{col} = 4.117 m; N_{col} = 24, Ω ($p/q/r/s$) = 6/9/6/3; Q_F = 1.45 m^3/min; Q_S = 5.39 m^3/min
1b (SMB)	Max Rec_pX, Min Q_D	same as Problem 1a except $5 \le p, r \le 8, 1 \le s \le 4$	Rec_pX $\ge$ 92%, Pur_pX $\ge$ 98%	same as Problem 1a except p, r, s are decision variables
1c (SMB)	Max Rec_pX, Min Q_D	same as Problem 1a except $6 \le p, r \le 9, 2 \le s \le 5$	Rec_pX $\ge$ 92%, Pur_pX $\ge$ 98%	same as Problem 1a except N_{col} = 28 and p, r, s are decision variables
2 (Varicol)	Max Rec_pX, Min Q_D	same as Problem 1a except Ω has 32 possible combinations	Rec_pX $\ge$ 92%, Pur_pX $\ge$ 98%	same as Problem 1a except p, r, s are decision variables
3 (SMB)	Max Rec_pX, Max Pur_pX	same as Problem 1b	Rec_pX $\ge$ 92%, Pur_pX $\ge$ 98%	same as Problem 1a except p, r, s are decision variables

a large number of simulations (often >2500 simulations, consisting 50 chromosomes for 50 generations). In such a scenario, it is very important that we use a simulation method that is less time-consuming. The results shown in the next section are obtained by using either of these methods. The MOL method was used in solving the case 1 optimization problem, whereas the OCFE method was used in solving the optimization problems described in cases 2 and 3.

Optimization of the SMB and Varicol Systems

It is quite well-known that one of the most serious problems associated with chromatographic processes is that, although they are efficient in separation, the resultant product streams are dilute, because of the high desorbent requirement. Even if the desorbent is inexpensive, it is desirable to have concentrated product streams, because dilute streams result in higher operational cost (viz. heat requirement) in the subsequent downstream separation processes, such as distillation. Moreover, as can be seen from Table 1, the operating flow rates are very high; as a result, the downstream separation processes would have to handle high volumes of material and, therefore, would be very energy-intensive. Therefore, reducing the desorbent consumption can help in regard to improving the economics of the overall process. Hence, one of the intents for the optimization of the Parex process is to improve the *p*-xylene recovery while reducing the total desorbent (*p*DMB) consumption.

In this work, a few two-objective function optimizations have been performed. Note that there is no end to the variety of multiobjective optimization problems that could be formulated and studied. In this article, only a few simple examples have been addressed, to illustrate the concept, technique, and interpretation of results. One can, of course, consider more than two-objective functions but the analysis of those results becomes cumbersome, because one must involve Pareto surfaces. In this study, a new state-of-the-art optimization technique based on Genetic Algorithm, which is a binary coded Nondominated Sorting Genetic Algorithm with Jumping Genes (NGSA-II-JG),[30] is utilized, which is an add-on novelty in the field of evolutionary algorithms[24] and allows handling of these complex optimization problems. In addition to the sorting and sharing mechanism introduced in the Elitist Nondominated Sorting Genetic Algorithm (NSGA-II),[31] which is the recent modification with jumping genes,[30] improves the diversity of the mating pool, leading to a much better spreading of solution at increased convergence speed. The jumping gene operations are performed by a macro−macro-mutation operator, and the concept is borrowed from the working of jumping genes (or transposons) in natural genetics. McClintock[32] suggested in the 1940s that jumping genes are DNAs that could jump in and out of chromosomes and can generate genetic diversity in natural populations, which is exploited in NSGA-II-JG. Details of the methodology and applications of different adaptations of NSGA-I in chemical engineering can be obtained elsewhere.[33]

In all optimization runs presented in this work, 50 chromosomes (solutions) were considered and results are presented after 50 generations. Note that optimization problems involved continuous variables such as column length, flow rates and switching, and discrete variables such as number of columns and their distribution in various sections. Several optimization problems were formulated and solved to determine the optimal operating conditions of the SMB for this *p*-xylene separation. Table 3 describes the list of the optimization problems solved in this study.

Problem 1a: Determination of Optimal Column Length (L_{col}). The first multiobjective optimization problem solved is maximization of the recovery of *p*-xylene (Rec_pX) with simultaneous minimization of the desorbent consumption (Q_D). To compare our results with those of Minceva and Rodrigues,[22] we fixed the diameter (d_{col}) and total number of columns (N_{col}), the number of columns in each section ($\Omega = p/q/r/s$), the feed flow rate (Q_F) and its concentration, the flow rate in section S (Q_S), and temperature (T), as given in Table 1. Four decision (manipulative) variables were used, namely, the raffinate (Q_{Ra}) and the desorbent (Q_D) flow rates, the switching time (t_s), and length of each column (L_{col}). Only four flow rates can be selected freely; the other four are determined by mass balance around nodes A−D (see Figure 1). Therefore, the remaining two flow rates were used as decision variables, namely, the raffinate (Q_{Ra}) and the desorbent (Q_D) flow rates. The third decision variable is the switching time t_s, which clearly has a strong influence on the performance of the SMB system. The bounds for t_s lie between the breakthrough times of the two components for the specific adsorbent. The fourth decision variable used is the length of each column L_{col}, because it is impossible to determine the optimal column length only through simulation. The optimization formulation and the bounds of the decision variables are summarized in Table 3 (see Problem 1a). It is to be noted that a very narrow range is used for the bounds. This is required to obtain meaningful optimum solutions, because of the existence of narrow "windows" for the decision variables. Such boundaries can be estimated very conveniently using equilibrium theory and some preliminary sensitivity

analysis of the model.[34] The formulation can be mathematically represented as follows:

$$\text{Maximize:} \quad J_1 = \text{Rec\_pX}\ [t_s, Q_{Ra}, Q_D, L_{col}] \quad (12a)$$

$$\text{Minimize:} \quad J_2 = Q_D\ [t_s, Q_{Ra}, Q_D, L_{col}] \quad (12b)$$

which are subject to the conditions

$$\text{Rec\_pX} \geq 92\% \quad (12c)$$

and

$$\text{Pur\_pX} \geq 98\% \quad (12d)$$

and has the decision variables and fixed parameters of

$$1\ \text{min} \leq t_s \leq 2\ \text{min} \quad (12e)$$

$$2\ \text{m}^3/\text{min} \leq Q_{Ra} \leq 3\ \text{m}^3/\text{min} \quad (12f)$$

$$2\ \text{m}^3/\text{min} \leq Q_D \leq 3.5\ \text{m}^3/\text{min} \quad (12g)$$

$$1\ \text{m} \leq L_{col} \leq 1.15\ \text{m} \quad (12h)$$

$$d_{col} = 4.117\ \text{m} \quad (12i)$$

$$N_{col} = 24 \quad (12j)$$

$$\Omega = 6/9/6/3 \quad (12k)$$

$$Q_F = 1.45\ \text{m}^3/\text{min} \quad (12l)$$

$$Q_S = 5.39\ \text{m}^3/\text{min} \quad (12m)$$

$$T = 453\ \text{K} \quad (12n)$$

The SMB model equations are given by eqs 1−9.

The inequality constraints on recovery and purity (eqs 12c and 12d) were imposed to restrict optimal solutions that satisfy at least the minimum (industrial) acceptable productivity and purity values. The optimization problem was solved using an adaptation of Genetic Algorithm, the Elitist Nondominated Sorting Genetic Algorithm with Jumping Genes (NSGA-II-JG), which was discussed previously. Details of the algorithm are available elsewhere.[30]

The Pareto optimal solution, along with the set of optimal decision variables, are shown in Figure 4. The figure clearly shows that the points do, indeed, constitute a Pareto set, i.e., as the recovery of *p*-xylene (Rec_pX) increases (desirable), the requirement for solvent (Q_D) also increases (undesirable). All points on this curve are equally good (nondominated) optimal solutions. The optimum length of each column (L_{col}) was determined to be 1.086 m, which is lower than the industrial operating point (1.134 m). For $Q_D = 2.89$ m^3/min, L_{col} was reduced by 0.048 m, which amounts to ca. 15.34 m^3 of total adsorbent savings for a 24-column SMB system. The optimum values of t_s were determined to be smaller, ~1.11 min, because of the reduction in the optimal column length, whereas the optimal value of Q_{Ra} was obtained as 7 m^3/min. The purity of *p*-xylene (Pur_pX) was observed to be almost the same as that obtained for the industrial operating point (~98.93%), for a recovery of 98.18%.

Problem 1b: Determination of Optimal Column Configuration (Ω). The optimal column distribution (configuration) and the number of columns (*p*, *q*, *r*, and *s*) in each section, viz., P, Q, R, and S (see Figure 1) determine the amount of adsorbent allocated for each section to conduct the required adsorption (or desorption) phenomenon. Hence, it is quite apparent that they also have a very important role in improving the recovery and purity of the desirable product. Optimal column distribution was determined while maintaining a value of $N_{col} = 24$ for the same optimization problem as in Problem 1a, except that three additional decision variables (*p*, *r*, and *s*, the number of columns in sections P, R, and S, respectively) were used. Figure 5 compares the Pareto optimal solution between these two problems (Problem 1a and 1b). The figure shows the shift in Pareto when the 24 columns are distributed optimally, yielding better recovery using less desorbent. Moreover, the optimal column length was further reduced by 0.021 m, which amounts to a further reduction of 6.71 m^3 of total adsorbent. The purity obtained in this case is slightly better, as shown in Figure 5. The optimum

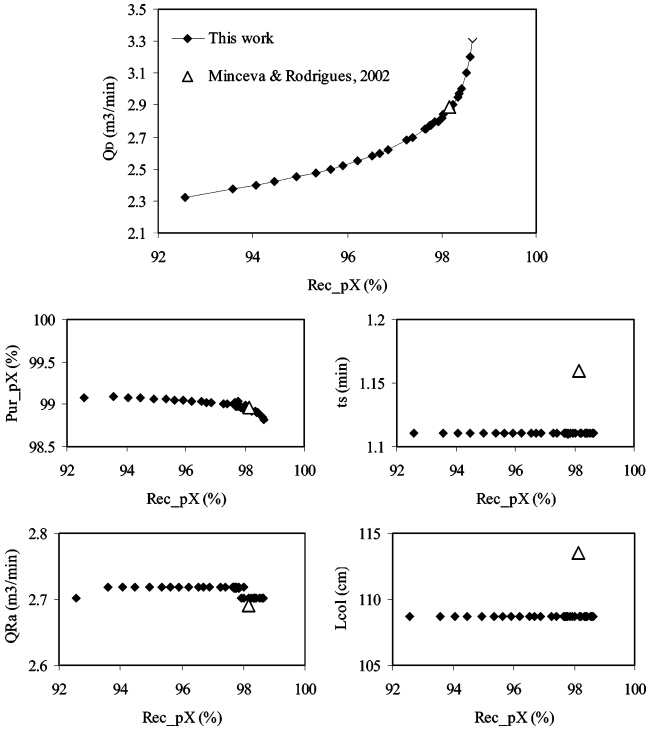

Figure 4. Pareto optimal solution and corresponding decision variables for Problem 1a.

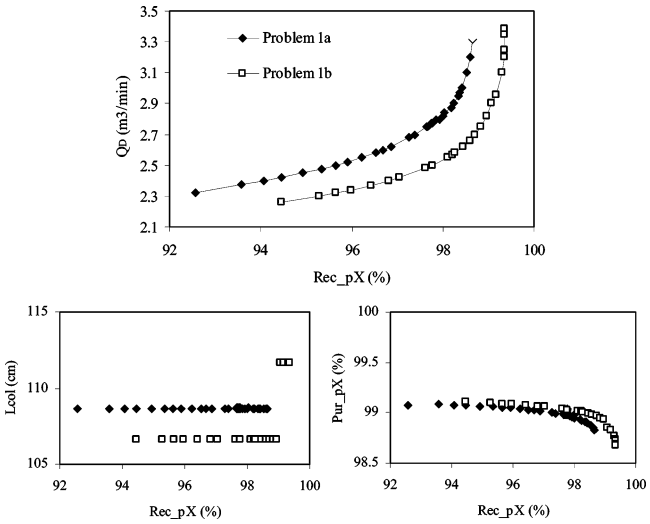

Figure 5. Comparison of Pareto optimal solution and corresponding decision variables for Problems 1a and 1b.

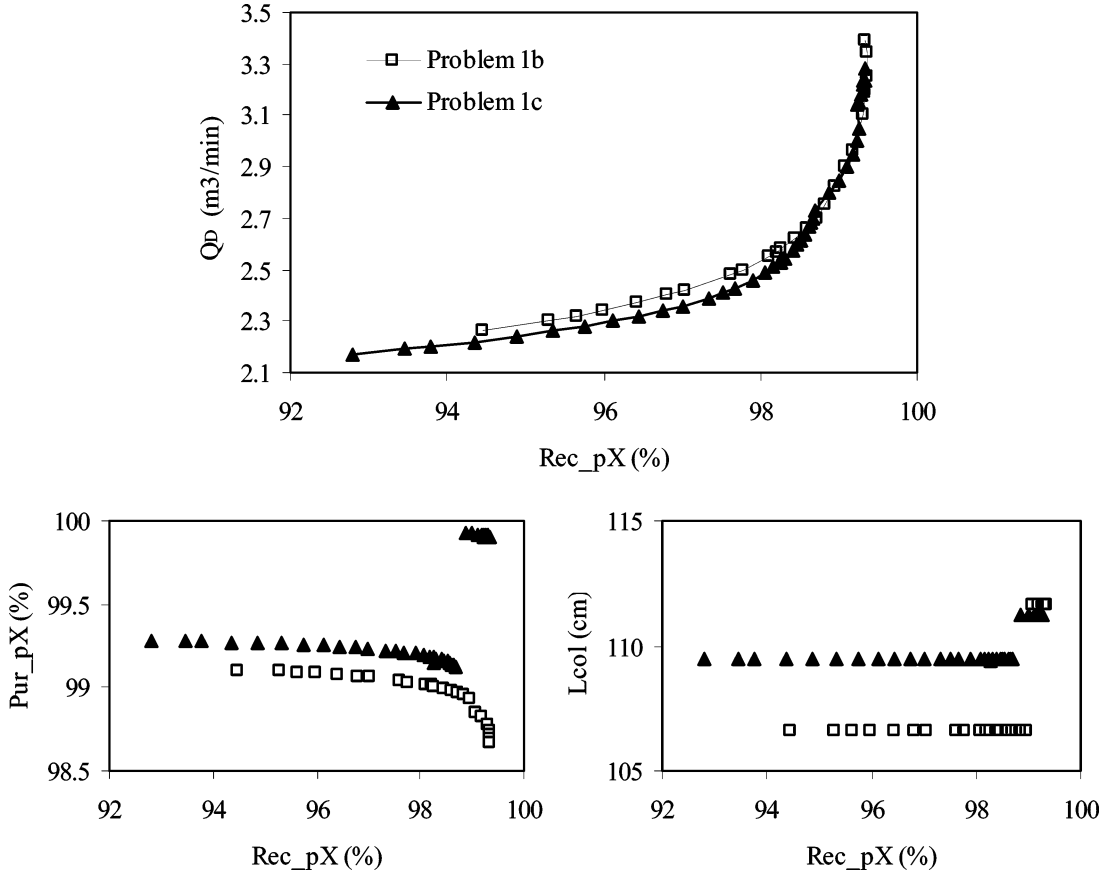

Figure 6. Comparison of Pareto optimal solution and corresponding decision variables for Problems 1b and 1c.

column configuration (Ω) was determined to be 7/6/7/4 for lower Q_D range, whereas a value of Ω = 8/6/8/2 was observed for higher values of Q_D (compared to Ω = 6/9/6/3, which was used for the industrial operating point[22]). The optimal configuration implies that more adsorbent is needed in sections P and R. Sections P and R involve, respectively, the desorption and adsorption of the strongly adsorbing component (*p*-xylene). Hence, for higher recovery and purity of the desired product (*p*-xylene) at a lower desorbent flow rate (Q_D), more solid adsorbent is required.

Problem 1c: Determination of Optimal Number of Columns (N_{col}). In some cases, there is a possibility of achieving better performance by increasing the total number of columns (N_{col}) but having a reduced length (L_{col}). This is possible because more columns would provide additional flexibility for operation. Hence, a new optimization problem with N_{col} = 28 was formulated and solved to determine if better performance can be achieved, compared to the 24 columns used in Problems 1a and 1b. Figure 6 compares the Pareto optimal solution, which shows a marginal shift (improvement) in Pareto, although there is slight increase in the purity of *p*-xylene (for example, Pur_pX = 99.12% when N_{col} = 28, compared to 98.96% for the 24-column SMB system for Rec_pX = 98.7%). However, the results show that 24 probably is the optimum number of columns and with further addition of columns, the improvement in the performance of the system is insignificant.

Problem 2: Comparison of the Performances between the SMB and Varicol Systems. Ludemann-Hombourger et al.[3] showed experimentally that the Varicol system can perform better than its equivalent SMB system, because of the flexibility in its operation. It could even aid in the reduction of the total volume of the adsorbent required. Hence, the optimization study was extended to a four-sub-interval, 24-column Varicol system to determine the extent of improvement that can be achieved over an equivalent 24-column SMB system. With N_{col} = 24 in the Varicol unit, there would be a very large number of possible column configurations. To reduce the computation time, extensive simulation studies were performed to determine the configurations that would lead to better performance of the system. From the results of the simulation study, 32 possible configurations were selected for the optimization study that could lead to better values of the objective functions. The optimization formulation is provided in Table 3 (Problem 2).

The Pareto optimal solution of the 24-column Varicol system is compared with the equivalent 24-column SMB system in Figure 7. The figure clearly shows that 100% recovery of *p*-xylene is possible, using a reasonable amount of eluent, and it evidently elucidates the performance improvement in the Varicol process, because of its greater flexibility, compared to the rigid SMB system. For example, for Q_D = 2.57 m^3/min, the Varicol process shows almost 100% recovery, whereas SMB shows only 98.21% recovery of *p*-xylene. Furthermore, the optimal L_{col} is further reduced by 0.054 m, which helps in achieving a further reduction of ~17.36 m^3 of adsorbent, which is remarkably high. The optimum switching time (t_s) obtained was 1.05 min. The optimal column configuration for the entire range of Pareto for the Varicol system was determined to be a grouping of five different combinations of column distribution, which is listed in Table 4. Three different optimal column configurations for the four-sub-interval,

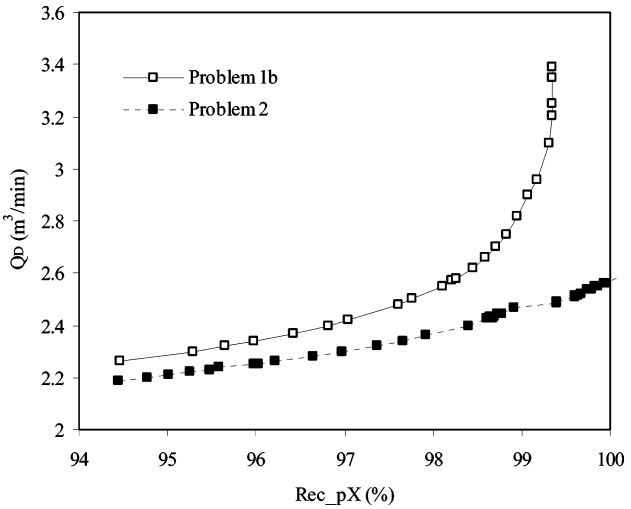

Figure 7. Comparison of Pareto optimal solution for Problem 1b (SMB process) and Problem 2 (Varicol process).

Table 4. Optimum Column Configurations[a] (Distribution) for $N_{col} = 24$

Ω	column configuration
A	8/5/7/4
B	5/8/8/3
C	7/6/8/3
D	8/5/8/3
E	8/4/8/4

[a] Column distribution Ω = A implies the number of columns in sections P, Q, R, and S are 8, 5, 7 and 4, respectively, for the SMB. Column distributions Ω = B, D, A, and E have the following implications for the Varicol process: $t/t_s = 0-0.25$ for Ω = B; $t/t_s = 0.25-0.5$ for Ω = D; $t/t_s = 0.5-0.75$ for Ω = A; and $t/t_s = 0.75-1$ for Ω = E. Note that only the optimal column configuration is shown here out of many possible column distributions for $N_{col} = 24$.

24-column Varicol system were obtained. For the lower desorbent flow rate region (Q_D < 2.23 m^3/min), the optimal configuration obtained was B-D-A-E, which means the following: for the first sub-time interval ($0-{}^1/_4 t_s$), the column distribution is B [≡ 5/8/8/3]; for the second sub-time interval (${}^1/_4 t_s - {}^1/_2 t_s$), the column distribution is D [≡ 8/5/8/3]; for the third time interval (${}^1/_2 t_s - {}^3/_4 t_s$), the optimal column distribution is A [≡ 8/5/7/4]; and for the last sub-time interval (${}^3/_4 t_s - t_s$), the optimal column distribution is E [≡ 8/4/8/4]. For 2.23 m^3/min < Q_D < 2.43 m^3/min, the optimal configuration obtained was B-A-A-E, whereas for Q_D > 2.43 m^3/min, the optimal configuration obtained was B-A-C-E. These configurations imply that, to increase the recovery of *p*-xylene while satisfying the desired purity constraint, sections P and R always require more columns. This can be easily understood by recalling the earlier discussion for Problem 1b, that these sections involve the adsorption and desorption of *p*-xylene and, hence, require more solid adsorbents.

Problem 3: Simultaneous Maximization of the Purity and Recovery of *p*-Xylene. In Problems 1 and 2, simultaneous maximization of *p*-xylene recovery with a minimization of desorbent consumption was studied. In this problem, both the recovery and purity of *p*-xylene are maximized simultaneously. Such types of multiobjective problems have been solved earlier,[7,25] and it has been observed that these two objective functions always contradict each other. The decision variables and their bounds used for this case are same as those considered for Problem 1b. A mathematical description of this problem is given in Table 3. The Pareto optimal solution is shown in Figure 8. The figure shows that the Pareto is very sensitive near the region of high *p*-xylene recovery. For *p*-xylene recovery from 92% to ~98.8%, the purity of *p*-xylene remains very high (~100%). Beyond this recovery value, the purity decreases very sharply and decreases to as low as 98.6% for a *p*-xylene recovery value of 99.5%. The corresponding optimal decision variables are also shown in Figure 8. Optimal Q_{Ra} values are constant at low recovery values but slowly decrease at higher values of *p*-xylene recovery. The optimal values of Q_D steadily increase as the *p*-xylene recovery increases but become insensitive to the maximization of objective functions thereafter. Hence, the plot of Q_D shows scattered points at higher *p*-xylene recovery values. It is observed that few variables (particularly Q_D) show insensitivity toward objective function values as long as Q_D above a minimum value is provided. However, the switching time t_s and the length of each column L_{col} are related. Therefore, multiple combinations can lead to the same objective function values. When the number of decision variables is increased, the decision variable plots become significantly scattered, in comparison to the smooth variation of the Pareto. The reason behind the scatter (which normally depicts a lesser influence of the variable on the objectives) is a compensating effect of the decision variables to generate similar, or the same, objective values.[36] This has recently been discussed.[37]

The optimum column length varies according to the recovery of *p*-xylene; however, the most dominating value of L_{col} chosen was ~1.05 m and the optimum t_s chosen was that according to L_{col}. The optimum column configurations obtained were Ω = 5/7/8/4 for the lower recovery values and Ω = 8/4/8/4 for the higher range of *p*-xylene recovery. The desorbent consumption in this case is certainly higher than that in earlier cases (Problems 1−2), because Q_D is not one of the objective functions in this case and certainly, to maximize purity, one needs higher desorbent flow rates. For example, for Problem 1b, the desorbent requirement was only 2.58 m^3/min for a recovery of 98.26%, whereas for this case, the value of Q_D needed was 2.93 m^3/min for the same recovery. However, the purity is now 99.95%, as compared to 99.0% for Problem 1b for the same recovery. Figure 9 compares the concentration profile between Problem 1b and Problem 3 for a *p*-xylene recovery of 98.26%.

Prediction of the Separation Regions and the Process Performance from Equilibrium Triangle Theory

To understand the reliability of the optimization results, it is worthwhile to discuss the results using equilibrium triangle theory[35] applied to counter-current chromatography. Storti et al.[35] showed that the unit behavior can be explained in terms of the flow rate ratio parameters relative to the four zones of the unit (see Figure 1):

$$m_\varphi = \frac{Q_\varphi^{SMB} t_s - V_{col}\epsilon}{V_{col}(1-\epsilon)} \qquad (\text{for } \varphi = \text{P, Q, R, S}) \quad (13)$$

In particular, the flow rate ratio parameter (m_P) must be larger than a critical value to achieve complete regeneration of the solid phase from the strongly adsorbed component, whereas the value of m_S must be smaller than a critical value to achieve complete regen-

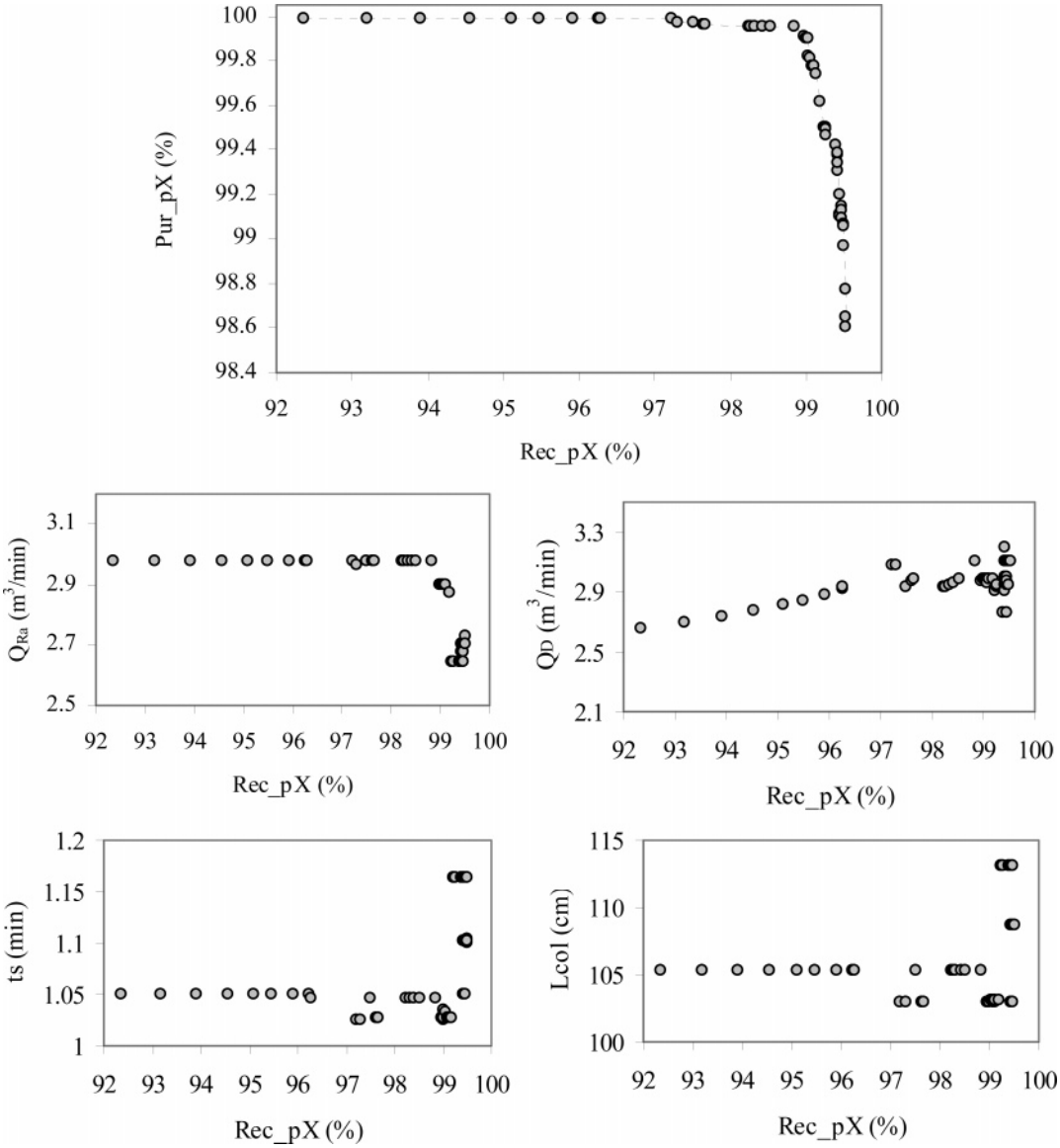

Figure 8. Pareto optimal solution and corresponding decision variables for Problem 3.

eration of the liquid phase from the weakly adsorbed component. When both of these conditions are satisfied, it is possible to identify in the m_Q-m_R parameter plane, which is a triangular region that includes all pairs of values leading to complete separation or where both components are recovered pure in the extract and in the raffinate, respectively. Also noteworthy is the fact that the distance from the diagonal of a point in the (m_Q-m_R) plane is directly proportional to the productivity and inversely proportional to the desorbent requirements. The vertex of the complete separation triangular region thus gives the optimal operating point, with respect to such process performance. This region is dependent only on the adsorption isotherms and the feed concentrations.

To interpret the results of the optimization, we have replotted the optimal values of the decision variables in Figure 4 for Problem 1b, in terms of the four flow rate ratio parameters m_φ (calculated from eq 13), as shown in Figure 10. This figure reveals that all operating points on the Pareto correspond to a substantially constant value of m_P, in agreement with the equilibrium theory that predicts a constant lower bound for such a parameter. We observe an increase in m_P only for the points corresponding to the higher recovery rate of *p*-xylene. This is due to the necessity to improve the solid regeneration in zone P to avoid the heavier component entering zone S and then polluting the raffinate. This also indicates that zone P is critical in controlling the recovery of *p*-xylene beyond a certain value. One must control the regeneration of the solid from the heavy component in zone P better. On the other hand, m_S undergoes smaller changes, indicating that zone S is much less critical to achieve the desired separation performance in the particular case under examination. It is seen that the values of m_Q and m_R obtained in each case change very little as the recovery rate increases. This is consistent with the equilibrium theory result, which indicates that the optimal operating point (the vertex of the triangle) is independent of the feed and eluent flow rates. Moreover, the values of m_Q and m_R should not vary greatly, according to equilibrium theory, which would see them constant and corresponding to the vertex of the complete separation region. However, because of dispersion phenomena, the same change in m_Q and m_R is observed, and, actually, they both have a tendency to decrease, as moving along the Pareto.

Figure 11 shows the m_Q-m_R plot. The diagonal $m_Q = m_R$ corresponds to a zero feed flow rate; therefore,

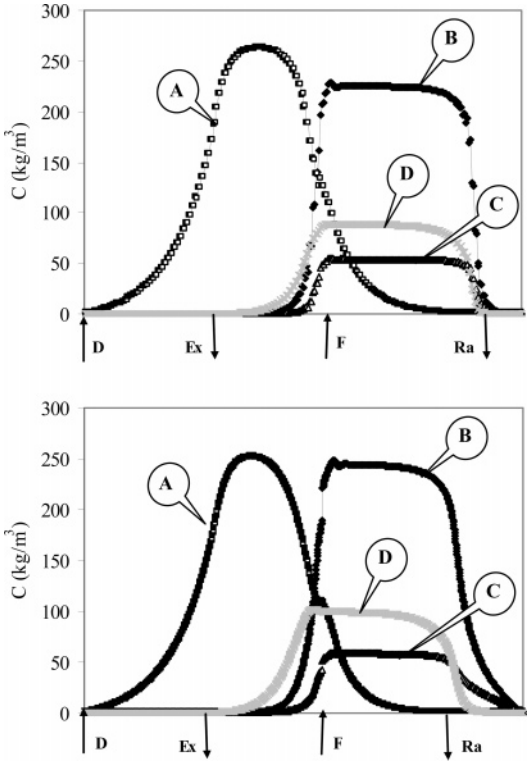

Figure 9. Comparison of steady-state concentration profiles for optimum points corresponding to Rec_pX = 98.26% shown in Figure 5 (Problem 1b) and in Figure 8 (Problem 3).

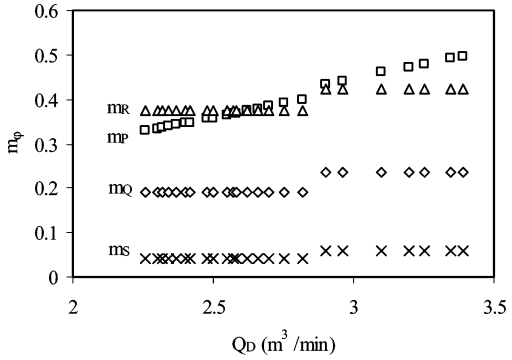

Figure 10. Calculated m_{φ} (see eq 13) values corresponding to Pareto optimal solutions shown in Figure 5 (Problem 1b).

m_R must be greater than m_Q when feed enters the system. The horizontal branch $m_R = 0.042$ (see Figure 10) corresponds to a zero raffinate flow rate. Hence, to obtain a point on the m_Q–m_R plane, the SMB model was successively solved for several values of m_Q and m_R within the region between the diagonal $m_Q = m_R$, the horizontal line $m_R = 0.042$, and the m_R-axis. The increment in m_Q used was 0.0125, which was chosen to be sufficiently small to provide precise determination of the separation region. For each pair (m_Q, m_R), the purity and recovery of *p*-xylene in the extract were also estimated. A high recovery of *p*-xylene in the extract implies high raffinate purity. The values that satisfy the constraints Pur_pX > 98% and Rec_pX > 92% were selected to build the region of pure separation. The values that did not fulfill this requirement were discarded. The region of pure separation calculated in this fashion is shown in Figure 11a. The vertex of the triangle provides the optimal operating conditions for the system. It corresponds to the point $m_Q = 0.1875$ and $m_R = 0.4625$ with Pur_pX = 98.9% and Rec_pX = 94.94%. Figure 11a was replotted (shown in Figure 11b) by further constraining the recovery of *p*-xylene, the points that were chosen were only those that correspond to Rec_pX > 98%. As can be seen in Figure 11b, the pure separation region narrows further. The vertex of the triangle now corresponds to the points $m_Q = 0.1875$ and $m_R = 0.3875$ with Pur_pX = 98.7% and Rec_pX = 98.5%. Note that this point is very similar to the values obtained from our optimization study ($m_Q = 0.19$ and $m_R = 0.38$).

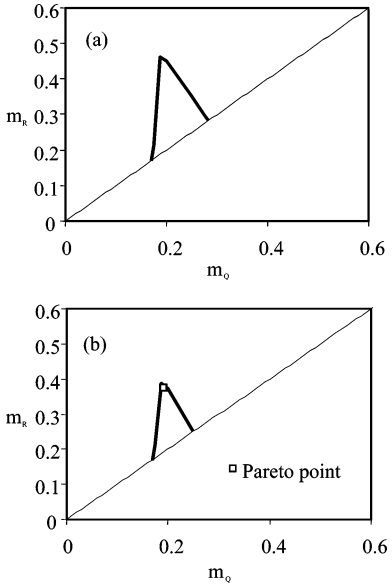

Figure 11. Optimal operating regimes in m_Q–m_R plane calculated from triangular theory for optimal solutions shown in Figure 10 (Problem 1b): (a) relaxed constraint and (b) stringent (restricted) constraint.

Conclusions

Continuous large-scale chromatographic separations of C_8 aromatics mixtures to recover *p*-xylene using simulated moving bed (SMB) technology have been of great interest for many years. In this paper, we have presented a systematic study for optimal operation of the SMB and Varicol processes for the recovery of *p*-xylene, based on the Parex process. The selection of operating parameters such as length and number of columns, switching time interval (in SMB) and sequence (in Varicol), and liquid flow rates in different sections is not straightforward. In most cases, conflicting requirements and constraints govern the optimal choice of the decision (operating or design) variables. In addition, SMB (and Varicol) systems for *p*-xylene recovery operate at high feed concentrations, which lead to nonlinear competitive adsorption behaviors.

The economical operation of the SMB (and Varicol) process is governed by many factors, depending on the objective and product quality. One may be interested in higher recovery of the desired component using minimum solvent (eluent) or may be interested in simultaneous maximization of recovery and purity of the desired product streams. In this paper, we have considered two multiobjective optimization problems that involve the simultaneous optimization of more than one objective function. Optimal design and operating conditions have been determined for two cases: (a) simultaneous maximization of *p*-xylene recovery with minimization of desorbent consumption, and (b) simultaneous maximization of productivity and purity of *p*-xylene. The

optimization has been performed using a very robust, AI-based technique called the Elitist Nondominated Sorting Genetic Algorithm with Jumping Genes (NSGA-II-JG). A Pareto optimal curve, which provides a set of optimal solutions that are equally good, is obtained for both the SMB and Varicol systems. It was determined that significant improvement could be obtained for SMB performance when column length and its distribution in various sections are selected appropriately. Moreover, Varicol process operation could lead to 100% *p*-xylene recovery, which is not possible with an equivalent SMB system. Systematic optimization resulted in better operating points, in terms of treating and recovering more *p*-xylene through the use of less eluent over the industrial operating point. Optimization results were also explained, using equilibrium theory.

Nomenclature

C = fluid phase concentration (kg/m^3)
D_{ax} = axial diffusivity (m^2/s)
d = diameter (m)
K = adsorption equilibrium constant (m^3/kg)
k_h = mass-transport coefficient (min^{-1})
L = length (m)
m = fluid-to-solid velocity ratios
N = number
Pe = Peclet number
Pur = purity (%)
q = adsorbed concentration averaged over the particle volume (kg/m^3)
$\bar{q}^*$ = concentration at the particle surface in equilibrium with bulk fluid (kg/m^3)
q_m = adsorbed phase saturation concentration (kg/kg of solid)
Q = flow rate (m^3/min)
R = radius of the pore (m)
Rec = recovery (%)
t = time (min)
T = temperature (K)
U_F = fluid interstitial velocity (m/min)

Greek Letters

α = number of mass-transfer units for a homogeneous adsorbent particle (LDF)
ν = solid-to-fluid volume ratio
χ = dimensionless length
ψ = dimensionless velocity
θ = dimensionless time
Ω = column configuration

Subscripts/Superscripts

col = column
D = desorbent, eluent, solvent
EB = ethylbenzene
Ex = extract
F = feed
i = species i
k = column k
NC = number of components
pX = *p*-xylene
Ra = raffinate
s = switching

Literature Cited

(1) Broughton, D. B.; Gerhold, C. G. Continuous Sorption Process Employing Fixed Bed of Sorbent and Moving Inlets and Outlets, U.S. Patent No. 2,985,589, 1961.

(2) Ruthven, D. M.; Ching, C. B. Countercurrent and simulated countercurrent adsorption separation processes. *Chem. Eng. Sci.* **1989**, *44*, 1011.

(3) Ludemann-Hombourger, O.; Nicoud, R. M.; Bailly, M. The "VARICOL" process: a new multicolumn continuous chromatographic process. *Sep. Sci. Technol*. **2000**, *35*, 1829.

(4) Zhang, Z.; Hidajat, K.; Ray, A. K.; Morbidelli, M. Multiobjective optimization of simulated moving bed system and varicol process for chiral separation. *AIChE J.* **2002**, *48*, 2800.

(5) Subramani, H. J.; Hidajat, K.; Ray, A. K. Optimization of simulated moving bed and varicol processes for glucose-fructose separation. *Chem. Eng. Res. Des.* **2003**, *81*, 549.

(6) Yu, W.; Hidajat, K.; Ray, A. K. Optimization of reactive simulated moving bed and varicol systems. *J. Chem. Technol. Biotechnol*. **2003**, *78*, 287.

(7) Subramani, H. J.; Hidajat, K.; Ray, A. K. Optimization of reactive SMB and Varicol system. *Comput. Chem. Eng*. **2003**, *27*, 1883.

(8) Fabri, J.; Greaser, U.; Simo, T. A. Xylenes production, separation and further processing. In *Ullmann's Encyclopedia of Industrial Chemistry*; Wiley−VCH GmbH: Weinheim, Germany, 2001.

(9) Santacesaria, E.; Morbidelli, M.; Danise, P.; Mercenari, M.; Carra, S. Separation of Xylenes on Y-Zeolite. 1. Determination of the adsorption equilibrium parameters, selectivities and mass transfer coefficients through finite bath experiments. *Ind. Eng. Chem. Process Des. Dev*. **1982**, *21*, 440.

(10) Santacesaria, E.; Morbidelli, M.; Servida, A.; Storti, G.; Carra, S. Separtion of Xylenes on Y-Zeolite. 2. Breakthrough curves and their interpretation. *Ind. Eng. Chem. Process Des. Dev.* **1982**, *21*, 446.

(11) Carra, S.; Santacesaria, E.; Morbidelli, M.; Storti, G.; Gelosa, D. Separtion of Xylenes on Y-Zeolite. 3. Pulse curves and their interpretation. *Ind. Eng. Chem. Process Des. Dev.* **1982**, *21*, 451.

(12) Azevedo, D. C. S.; Neves, S. B.; Ravagnani, S. P.; Cavalcante, C. V., Jr.; Rodrigues, A. E. The influence of dead zones of simulated moving bed units. In *Fundamentals of Adsorption 6*; Elsevier: Amsterdam, The Netherlands, 1998; p 521.

(13) Hsiao, H. S.; Yih, S. M.; Li, M. H. Adsorption equilibrium of xylene isomers and *p*-diethylbenzene in the liquid phase on a Y-zeolite. *Adsorpt. Sci. Technol*. **1989**, *6*, 64.

(14) Santacesaria, E.; Geloza, D.; Danise, P.; Carra, S. Separation of Xylenes on Y-Zeolite in the Vapor Phase. 1. Determination of the Adsorption Equilibrium Parameters and of the Kinetic Regime. *Ind. Eng. Chem. Process Des. Dev*. **1985**, *24*, 78.

(15) Morbidelli, M.; Santacesaria, E.; Storti, G.; Carra, S. Separation of Xylenes on Y-Zeolite in the Vapor Phase. 2. Breakthrough and Pulse Curves and Their Interpretation. *Ind. Eng. Chem. Process Des. Dev.* **1985**, *24*, 83.

(16) Storti, G.; Santacesaria, E.; Morbidelli, M.; Carra, S. Separation of Xylenes on Y-Zeolite in the Vapor Phase. 3. Choice of the Suitable Desorbent. *Ind. Eng. Chem. Process Des. Dev*. **1985**, *24*, 89.

(17) Ruthven, D. M.; Goddard, M. Sorption and diffusion of C_8 aromatic hydrocarbons in Faujasite type zeolites. I. Equlilbrium isotherms and separation factor. *Zeolites* **1986**, *6*, 275.

(18) Goddard, M.; Ruthven, D. M. Sorption and diffusion of C_8 aromatic hydrocarbons in Faujasite type Zeolites. II. Sorption kinetics and intracrystalline diffusivities. *Zeolites* **1986**, *6*, 282.

(19) Paludetto, R.; Storti, G.; Gamba, G.; Carra, S.; Morbidelli, M. On Multicomponent Adsorption Equilibria of Xylene Mixture on Zeolite. *Ind. Eng. Chem. Res.* **1987**, *26*, 2250.

(20) Cavalcante, C. L., Jr.; Lima, V. E.; Sousa, L. G.; Alsina, O. L. S. Sorption kinetics of aromatics in Y-zeolite pellets using the gravimetric method. *Braz. J. Chem. Eng*. **1997**, *14*, 191.

(21) Storti, G.; Masi, M.; Carra, S.; Morbidelli, M. Optimal design of multicomponent countercurrent adsorption separation processes involving nonlinear equilibria. *Chem. Eng. Sci.* **1989**, *44*, 1329.

(22) Minceva, M.; Rodrigues, A. E. Modeling and simulation of a simulated moving bed for the separation of *p*-xylene. *Ind. Eng. Chem. Res*. **2002**, *41*, 3454.

(23) Bhaskar, V.; Gupta, S. K.; Ray, A. K. Applications of multiobjective optimization in chemical engineering. *Rev. Chem. Eng*. **2000**, *16*, 1.

(24) Deb, K. *Multi-objective Optimization Using Evolutionary Algorithms*; Wiley: Chichester, U.K., 2001.

(25) Zhang, Z.; Hidajat, K.; Ray, A. K. Multiobjective Optimization of Simulated Countercurrent Moving-Bed Chromatographic Reactor (SCMCR) for MTBE Synthesis. *Ind. Eng. Chem. Res*. **2002**, *41*, 3213.

(26) Yu, W.; Hidajat, K.; Ray, A. K. Application of multi-objective Optimization in the Design and Operation of Reactive SMB and Its Experimental Verification. *Ind. Eng. Chem. Res*. **2003**, *42*, 6823.

(27) Yan, Z.; Hidajat, K.; Ray, A. K. Optimal design and operation of SMB bioreactor: production of high fructose syrup by isomerization of glucose. *Biochem. Eng. J*. **2004**, *21*, 111.

(28) Pais, L. S.; Loureiro, J. M.; Rodrigues, A. E. Modeling strategies for the enantiomers separation by SMB chromatography. *AIChE J.* **1998**, *44*, 561.

(29) Ray, A. K.; Gupta, S. K. *Mathematical Methods in Chemical and Environmental Engineering*, 2nd Edition, Revised; Thomson Learning: Singapore, 2004.

(30) Kasat, R. B.; Gupta, S. K. Multiobjective optimization of an industrial fluidized bed catalytic cracking unit (FCCU) using genetic algorithm (GA) with the jumping genes operator. *Comput. Chem. Eng*. **2003**, *27*, 1785.

(31) Kasat, R.; Kunzru, D.; Saraf, D. N.; Gupta, S. K. Multi-objective Optimization of Industrial FCC Units Using Elitist Nondominated Sorting Genetic Algorithm. *Ind. Eng. Chem. Res*. **2002**, *41*, 4765.

(32) McKlintock, B. *The Discovery and Characterization of Transposable Elements—The Collected Papers of Barbara McKlintock*; Garland: New York, 1987.

(33) Nandasana, A. D.; Ray, A. K.; Gupta, S. K. Applications of the nondominated sorting genetic algorithm (NSGA) in chemical reaction engineering. *Int. J. Chem. Reactor Eng.* **2003**, *1* (R2), 1.

(34) Wongso, F.; Hidajat, K.; Ray, A. K. Optimal operating mode for enantioseparation of SB-553261 racemate based on SMB technology. *Biotechnol. Bioeng*. **2004**, *87*, 704.

(35) Storti, G.; Baciocchi, R.; Mazzotti, M.; Morbidelli, M. Design of Optimal Operating Conditions of Simulated Moving Bed Adsorptive Separation Units. *Ind. Eng. Chem. Res*. **1995**, *34*, 288.

(36) Tarafder, A.; Rangaiah, G. P.; Ray, A. K. Multiobjective optimization of an industrial styrene manufacturing process. *Chem. Eng. Sci*. **2005**, *60*, 347.

(37) Tarafder, A.; Rangaiah, G. P.; Ray, A. K. A study of neighbourhood multimodal multi-objective (nM3O) solutions in chemical process optimization. *Comput. Chem. Eng*. submitted, **2005**.

Received for review November 23, 2004
Revised manuscript received May 6, 2005
Accepted May 23, 2005

IE0488694